# Investigating the Effects of a Moving Surface on the Drag and Thermal Performance

Khaled M. K. PASHA
*Department of Mechanical Power Engineering, Modern University, Cairo, Egypt*

***Abstract:*** **- In the applications that include relative motion between a fluid and a solid body, the circulation bubbles in the body wake affect greatly the exerted thermal transport and drag on the body. In each studied case in the present work, we move part of the body surface and investigate the change in the drag and heat transfer from the fluid around this body. In some cases, we suggest rotating a cylinder that is mounted next to a backward-facing step located in the entrance to a duct. It is required to investigate the heat transfer and the drag on the cylinder, the step, and the wall downstream of the step. The investigation is executed with different values of Reynolds numbers, different cylinder rotation speeds, and different cylinder positions. The results showed that a maximum local Nusselt number value of 31.3 could be achieved at Reynolds number, Re, equals 400, when the cylinder is at height H, that equals half the step height, S and is rotating counterclockwise at rim speed, ω r, that equals five times the inlet velocity, $U_i$. The non-dimensional force on the step in the opposite flow direction achieved a maximum value of -0.103 with Re=400, H=1.0 S, and ω r=5 $U_i$. Another suggested case is to move a cylinder in the corner of a simulated bus, where, the drag was reduced by 7.3% when Re=6817, and $\omega_c = U_i/r$.**

***Keywords*****: moving surfaces, cylinder, backward step, drag, Nusselt**

## I. INTRODUCTION

For applications where there exists a relative motion between a solid body and a fluid, there are great considerations for the forces generated on the solid surfaces and the heat exchange between the fluid and the body. Many passive and active methods were suggested to alter the circulation bubbles in the body wake and consequently, to reduce the drag and increase the heat exchange.

### *1.1Theoretical investigation*

Choi et al. (2016), carried out a number of numerical simulations for various step angles, different expansion ratios, and different values of Reynolds numbers. They compared the flow structures, separation, and reattachment lengths. They verified that the reattachment length remains almost constant once Re > 15,000, even when increasing the step anglebeyond 30°. Wang et al. (2019), developed Large-eddy simulation (LES) and *κ-ε* models for a specific geometrical configuration of the backward-facing step (BFS). They reported that the LES model cannot effectively simulate the boundary layer near-wall areas without sufficiently fine grids and it tends to overestimate the top wall separation. Mushyam and Bergada (2015), analyzed two-dimensional flow over a backward-facing step in the laminar flow regime with the application of active flow control (AFC) technique. They used two different kinds of AFC techniques; zero net mass flow actuators and fluidic actuators. They observed that the maximum drag reduction occurred when using an AFC frequency ± 10% of the vortex shedding. Barkley et al. (2002), analyzed the three-dimensional computational stability of flow over a backward-facing step with an expansion ratio of 2 at Reynolds numbers between 450 and 1050. Their analysis shows that the first absolute linear instability of the steady two-dimensional flow is a steady three-dimensional bifurcation at a critical Reynolds number of 748. Lan et al. (2009), executed (3-D) simulations of turbulent forced convection adjacent to backward-facing step in a rectangular duct. They used three-dimensional backward-facing step geometry with an expansion ratio of 1.48 and with a step height of 4.8 mm and with three aspect ratios of 3, 8 and infinity (2-D simulation). They simulated several 2-D separated flow/heat transfer benchmark problems. The agreement of their 2-D model results and the published data suggested that it is possible to use this resource for simulating 3-D convection problems. Durst and Tropea (1982), presented experimental results of the mean and turbulence velocity fields for the flow over two-dimensional backward-facing steps in ducts for a Reynolds number range between 2 × 103 and $2 \times 10^4$. Within this range, the reattachment length exhibited large variation and it is related to the formation of large vortex structures in the separated shear layer. Durst and Pereira (1988), performed a numerical study of the impulsively starting backward-facing step flow for different values of Reynolds numbers. They reported that, for the higher Reynolds numbers, the flow starts to separate on the lower and upper corners of the step yielding two disconnected re-circulating flow regions for some time after the flow has been impulsively started. then, these two separated flow regions connect up and a single re-circulating flow region emerges. And for Reynolds number Re = 368, a separated flow region is observed and it is shown to occur for some finite time period of the developing, impulsively started backward-facing step flow. Slim et al. (1990), investigated the urbulent, incompressible duct flow over a backward-facing step with a very small aspect ratio. They found that the reattachment length in their case was considerably shorter than that of two-dimensional backward-facing step flow, and the propagation of strong stream-wise vortices was observed. Chen et al. (2018), reviewed the Backward-Facing Step

Flows, BFS in various experimental and numerical. they summarized the basic models and the parameter-based after-step flow laws. They reported that the step size (duct expansion ratio) will define the basic re-circulation and re-attachment process. Armaly et al. (1983), performed Laser-Doppler measurements of velocity distribution downstream of a backward-facing step in a two-dimensional channel for laminar, transitional and turbulent flow of air. They reported that there are additional regions of flow separation downstream of the step and on both sides of the channel test section, and the flow downstream of the step only remained two-dimensional at low and high Reynolds numbers. Choveta et al. (2017), studied the unsteady behavior of separated and reattaching flows over a backwardfacing for Reynolds numbers ranged from 31500 to 182600. They indicated that in the region close to the separation point, even for high Reynolds numbers, the low-frequency flapping motion is relatively dominant over the high-frequency mode of the large scale vortical structure. Ajeel et al. (2018), examined adiabatic conditions for the straight walls, constant heat flux for the corrugated walls, and zigzag configuration of semicircle corrugated channel. They showed that the zigzag profile of semicircle corrugated channel has a great effect on the thermal performance compared with a flat profile. Also, the Nusselt number dropped as the nanoparticle diameter grew. Srivastava et al. (2019), carried out a computational study to examine the effects of ribs and cavities on flow and heat transfer in a convergent-divergent shaped microchannel heat sink with constant heat flux. They showed that the usage of CD shape with ribs and cavities can reduce the overall thermal resistance up to 40%, also, can make the bottom surface temperature quite uniform. This heat transfer enhancement is mainly due to the interruption and redevelopment of boundary-layers along with the recirculation zone. They reported an enhanced heat transfer in terms of increased averaged Nusselt number from 15% to 46%.

Saravanan et al. (2018), presented a comparison of fluid flow and heat transfer characteristics for micro pin fin heat sink and microchannel pin fin heat sink for UN finned microchannel heat sink. They indicated that the microchannel pin fin heat sink has the highest Nusselt number and friction factor for all Reynolds number range. Also, the formation of secondary vortices enhances heat transfer in a microchannel heat sink with a square pin fin compared to a micro channel heat sink with circular pin fin. Bazgir and Nabhani (2018), optimized uniform and non-uniform cross section vortex tubes utilizing straight, convergent and divergent hot-tubes. They analyzed the axial angle of inlet nozzles, inlet pressure, mass flow rates and the number of inlet nozzles, and the inlet gas in order to optimize the cooling efficiency of the vortex tube (straight). They showed that utilizing the divergent hot-tubes increases the isentropic efficiency for all inlet pressure values. Djedai et al. (2017), performed a numerical study of active flow control using a blowing technique using steady and incompressible RANS (Reynolds averaged Navier- Stokes) equations and Realizable k-ε turbulence model. They found that the blowing slot should be located upstream the dual nature critical point where the origin of separation is expected. Also, the removal of the corner separation was not achieved by the slots on the blade suction side and on the end-wall. Rafiee and Sadeghiazad (2016), performed a numerical investigation to study the impacts of the length of the main (hot) tube (95 to 125 mm) and type of the boundary condition on the thermal capability (heating and cooling) of the vortex tube. They considered also the heat and mass transfer between the cold and hot vortex cores inside a Ranque-Hilsch vortex tube applying the 3D CFD models. Their model agreed with the experimental results with a deviation of about 7 %.

*1.2 The Objectives*

It is required to study the effects of surface movements on the transport of the thermal and momentum. The first part of the research includes the investigation of a cylindrical surface which is mounted next to a backward step of height equals, S at different heights, H and rotates clockwise and anticlockwise at different speeds, **ω**. Air is flowing at different Reynolds numbers through a tunnel whose lower wall is kept at a constant temperature. The second part is to investigate the effect of a rotating cylindrical surface on the drag that is exerted on a moving body.

## II. NUMERICAL PREPARATIONS

The domains were meshed using the code GAMBIT, and after different preliminary runs, it was found that, for all the investigated cases, the pave meshing scheme with the tri-element type gave the required fine mesh resolutions around the critical surfaces and coarser resolutions along with the directions away from these surfaces.

The studied cases are; the case without cylinder and another three cases in which, the cylinder is at heights equal 0.5S, 1.0S, and 1.5 S. The preliminary runs also revealed that the stable grid resolution required 392000, 572000, 520000, and 492000 elements for the cases; no cylinder, H=0.5S, H=1.0S, and H=1.5S, respectively. The numerical simulations were performed using ANSYS 14.5 with the solver 'pressure-based' and a standard k-epsilon model and wall function. The turbulent intensity and the turbulent viscosity ratio were limited by 4% and 0.8, respectively. In all the studied cases, the step has a height, S, which equals 2 cm. The air passage has a length of 50 S, the passage height equals S upstream the step, and equals 2S downstream the step. Figure 1 illustrates the meshed domains for the studied cases.

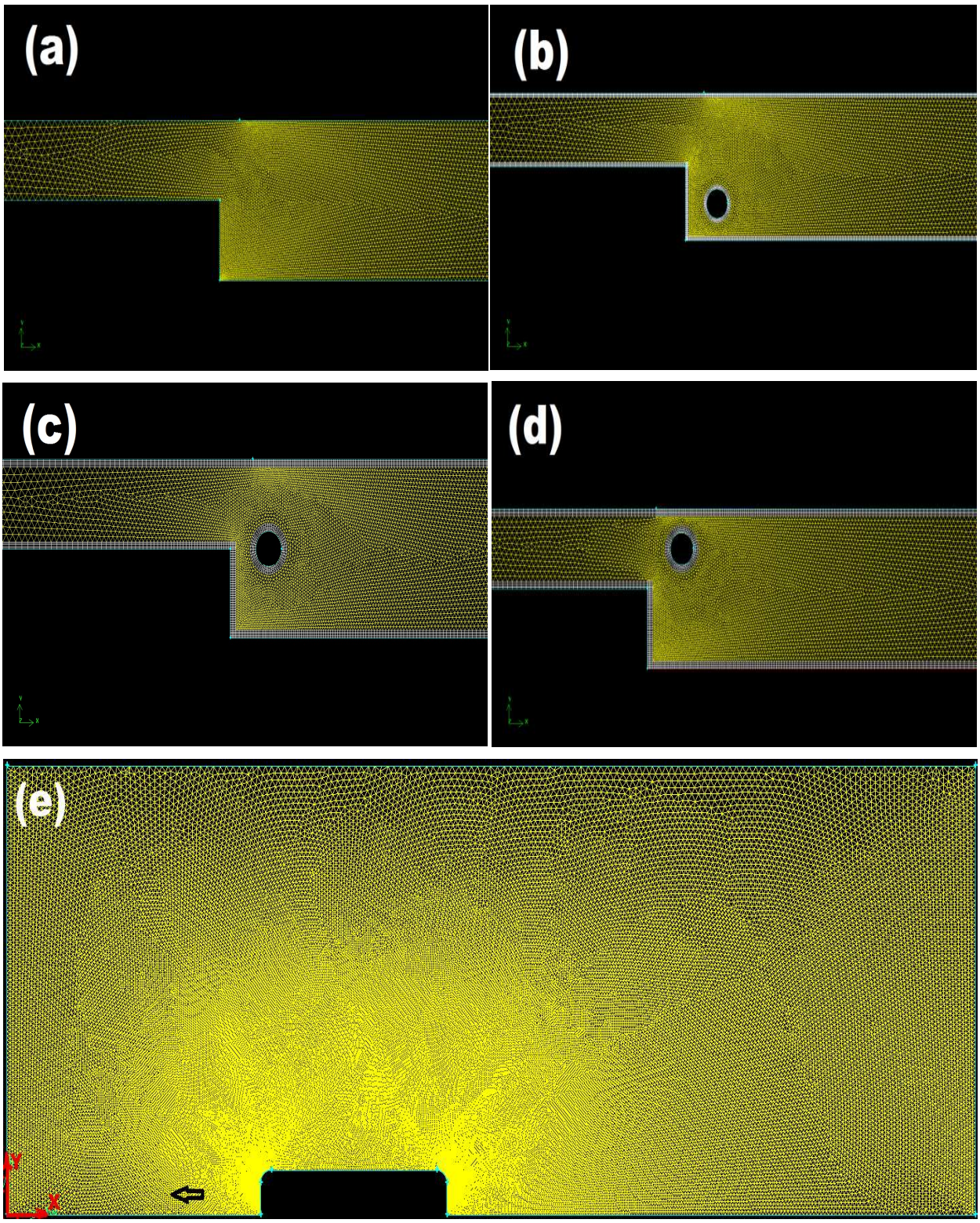


Fig. 1 the meshed domains for the studied cases;

a) Passage without cylinder. b) Cylinder at hight H= 0.5 S. c) Cylinder at hight H= 1.0 S.

d) The cylinder at hight H= 1.5 S. e) Passage with a moving body, (bus)

## III. RESULTS AND DISCUSSIONS

### *3.1 The forces on the different walls*

The positions and dimensions of both the step and the cylinder affect greatly the flow patterns, and accordingly, the pressure and shear distributions on the different domain walls. The component of the drag force on the cylinder wall in the flow direction consists of two components; the skin friction and the form drag, which results from the pressure distribution on the cylinder surface. The form drag in the flow direction is calculated from;

$$\boldsymbol{D_{form,x}} = \int \boldsymbol{p dA_x} \quad \textbf{(1)}$$

The drag in the flow direction due to the skin friction is calculated from;

$$\boldsymbol{D_{skin,x}} = \int \boldsymbol{\tau}_x \, \boldsymbol{dA} \quad \textbf{(2)}$$

And the total drag coefficient is;

$$\boldsymbol{C_D} = \frac{\boldsymbol{D_{form,x}} + \boldsymbol{D_{skin,x}}}{0.5\,\rho U_i^2 S} \quad \textbf{(3)}$$

And the Reynolds number, based on the step height, H, is ;

$$\boldsymbol{Re} = \frac{\rho U_i H}{\mu} \quad \textbf{(4)}$$

The flow field next to the step and around the cylinder is visualized in Fig. 2 for different cylinder heights, different rotation speeds, and at Reynolds number that equals 100. It is observed that, for H=0.5 S and **ω = 0,** the flow circulation appears next to the step, and almost disappear behind the cylinder. the presence of the cylinder in the region where the circulation due to the step is expected results in a momentum reduction that reduces the possibilities of pressure reduction and formation of circulation bubbles. That may lead to a pressure increase on the step and a pressure decrease the back surface of the cylinder, and accordingly, lower forces on the step and higher drag on the cylinder. For H=0.5 S and $\boldsymbol{\omega = U_i / r}$, the circulation direction of the flow adjacent to the cylinder strengthens the downward flow near the step which imparts the circulation there. The cylinder rotation also opposes the core flow which decreases the strength of circulation near the step. This action reduces the possibilities of pressure reduction near the step and accordingly, increases the force on it. In both the previous cases, the low momentum flow behind the cylinder does not promote higher total pressure on the cylinder back surface which means a lower drag on the cylinder.

For H=1.0 S and **ω =0,** the high-speed flow through the narrow passage between the cylinder and the step enforces the circulation bubble to move downward in the region of low-speed fluid and reduces its effect of reducing the pressure on the step. So, the pressure on the step is higher than that of the cylinder at H=0.5S. For H=1.0 S and ω = $U_i$, the cylinder rotation enforces the circulation bubble to move downward which promotes the increase of pressure forces on the step.

A large portion of the cylinder back surface is exposed to the high-speed flow, and the surface is rotating counter-clockwise direction such that, it receives higher skin friction from the faster fluid in the core. The back surface receives higher total pressure too, and so, this case has the highest cylinder drag.

For H=1.5 S and **ω = 0,** the flow passage behind the cylinder is wider which results in lower fluid speed in that region and promotes a circulation bubble near the step and accordingly, a lower pressure on the step. The whole back surface area of the cylinder is exposed to the flowing fluid but, the larger passage area between it and the step reduces the velocity gradient near the cylinder and accordingly, reduces the skin friction. So, the drag on the cylinder lower than that of the case H=1.0S and, larger than that of the case H=0.5S. For the case H=1.5 S and $\boldsymbol{\omega = U_i}$, although the rotation direction of the cylinder helps in pushing the flow downward but, the larger flow passage area still allows the formation of circulation bubbles which reduces the pressure forces on the step. The cylinder surface, that moves in an opposite direction to the main flow, produces a higher velocity gradient and accordingly larger skin friction than the case of H=S. Figure 3 illustrates the variations of the non-dimensional pressure force on the step with the Reynolds number at different cylinder positions and speeds of rotation. Figure 4 illustrates the effects of rotation speeds on the variations of the non-dimensional total drag on the cylinder at different level heights, and at Re = 200.

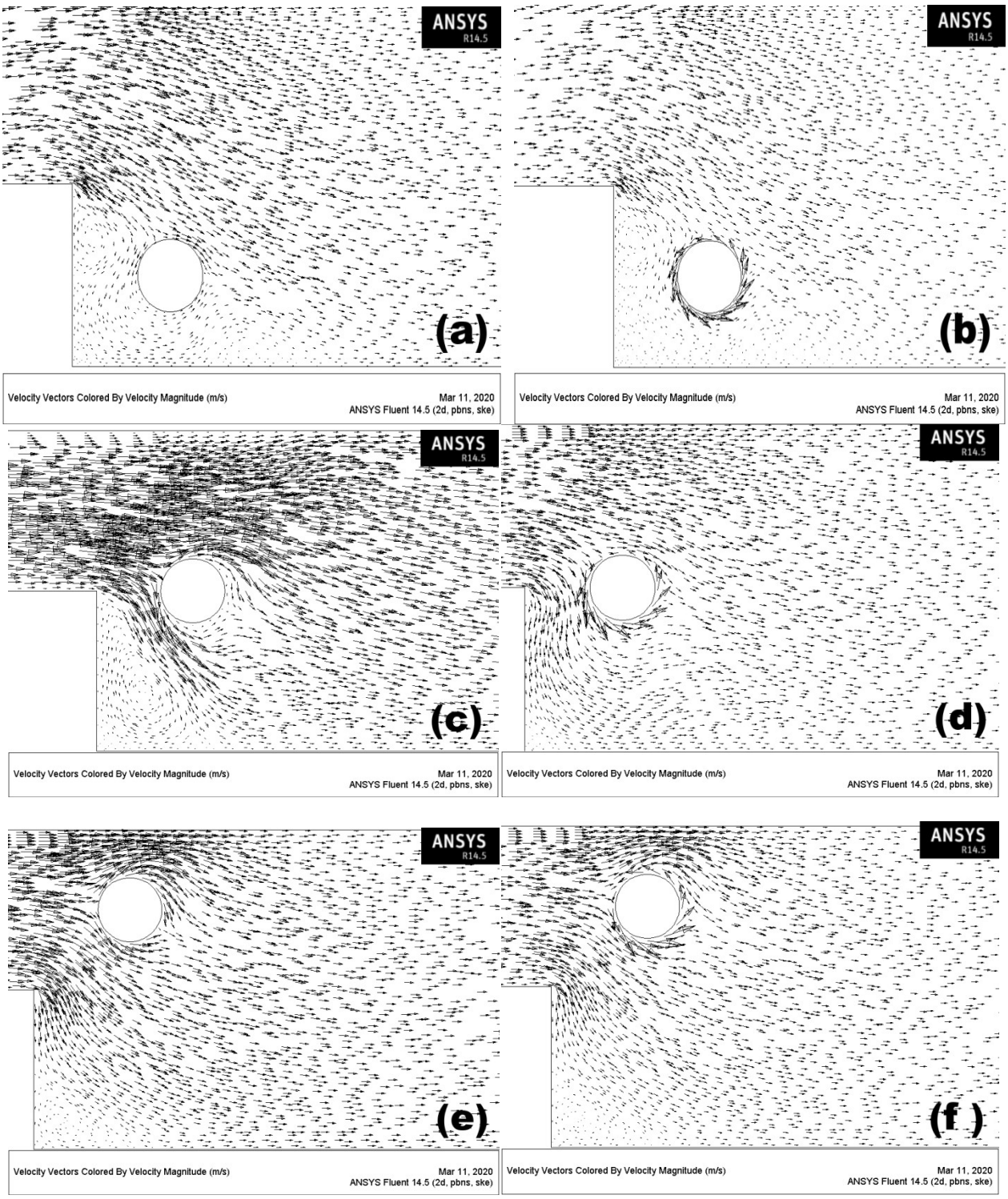


Fig. 2 the flow directions for different cases;

a) H= 0.5 S, Re = 100, and ω = 0.
b) H= 0.5 S, Re = 100, and ω = 5 $U_i$ / r.
c) H= 1.0 S, Re = 100, and ω = 0.
d) H= 1.0 S, Re = 100, and ω = 5 $U_i$ / r.
e) H= 1.5 S, Re = 100, and ω = 0.
f) H= 1.5 S, Re = 100, and ω = 5 $U_i$ / r.

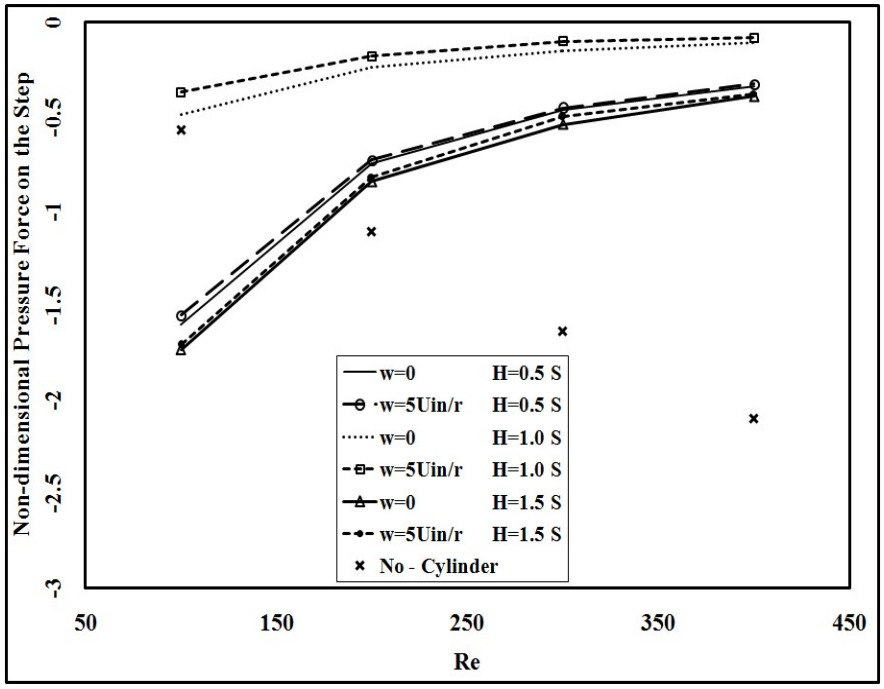


Fig. 3 the variations of the non-dimensional pressure force on the step with Reynolds number at different cylinder positions and speeds of rotation.

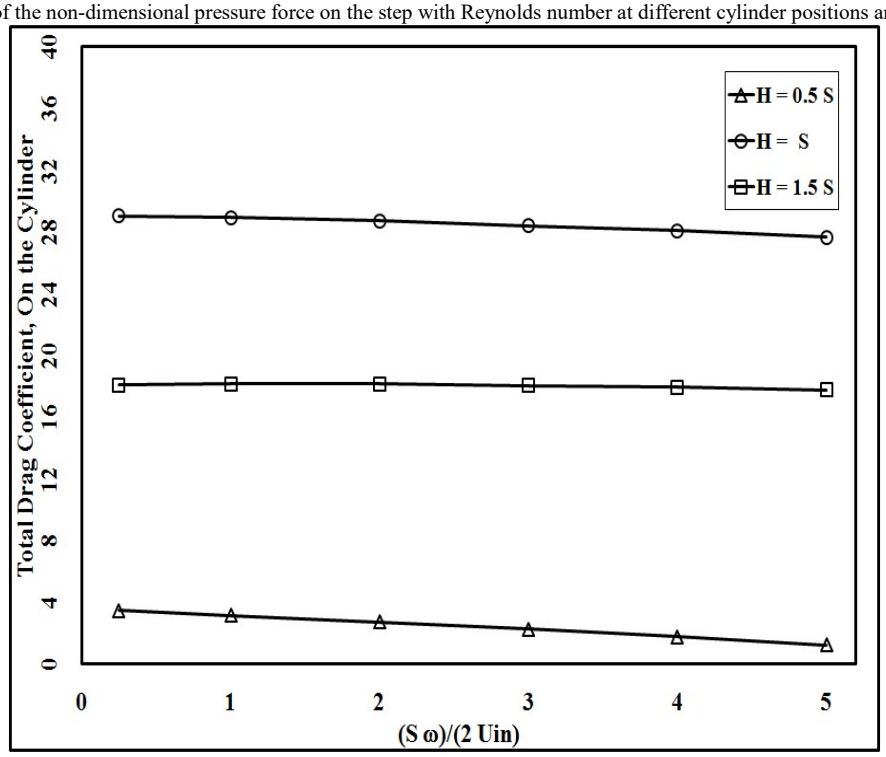


Fig. 4 the variations of the non-dimensional total drag on the cylinder at different level heights, and at Re = 200.

Next to the above, we simulated a real application, (a moving bus), in which, we investigated the effects of a moving surface on the force exerts on its back surface. This force supports the motion against the drag force. It is known that the location and strength of the circulation bubbles in the wake of a moving body affect greatly the pressure force on its back surface. So, we suggested putting a rotating cylinder in the upper right corner of a moving block that simulates a moving bus. Many preliminary runs.

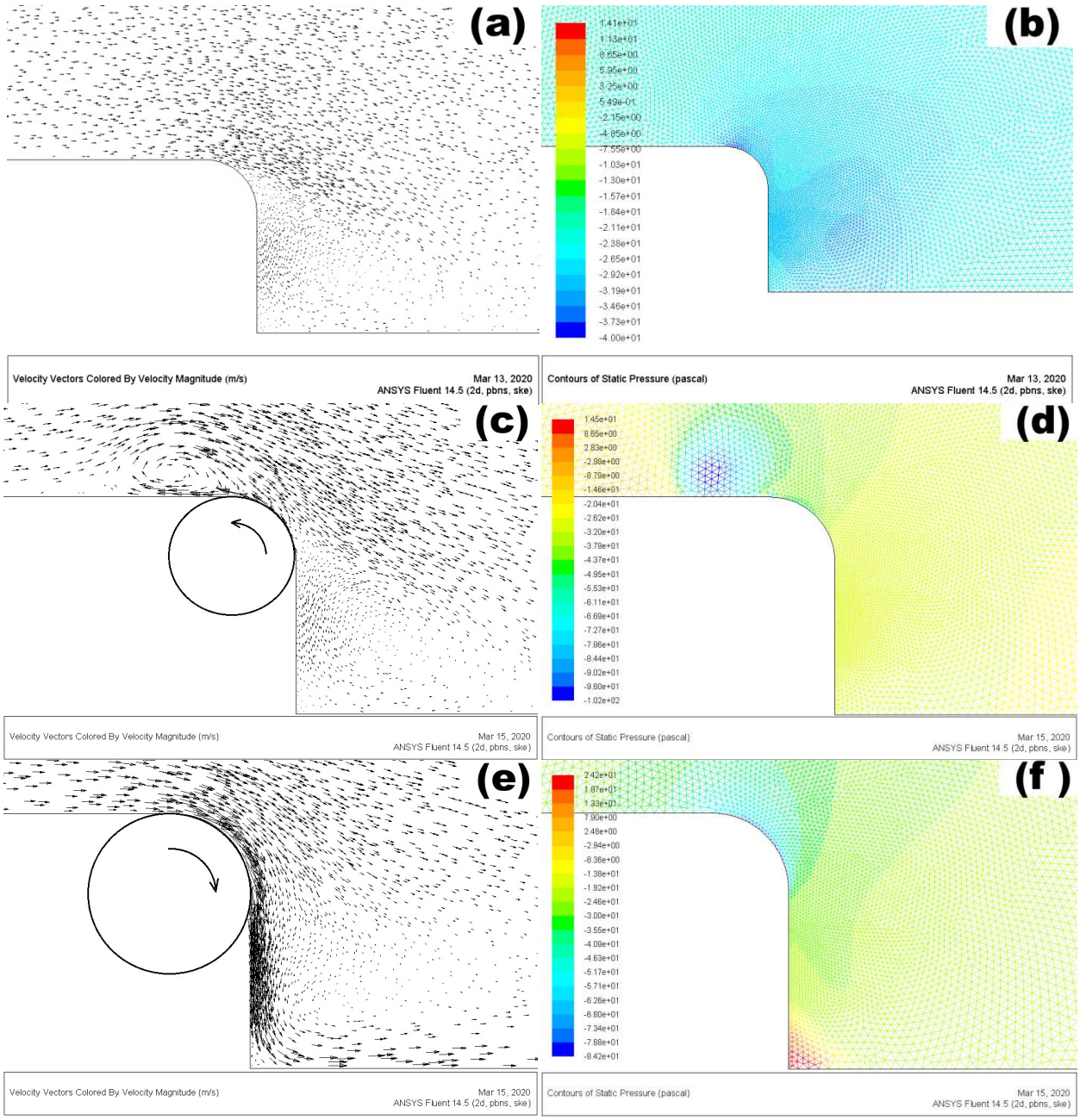


Fig. 5 the flow directions and the pressure distribution on a moving bus for different cases;

a) Flow around the moving bus, Re=6817, $\omega_c$ =0.
b) Pressure distribution on the moving bus, Re=6817, and $\omega_c$ = 0
c) Flow around the moving bus, Re=6817, and $\omega_c = U_i$ / r.
d) Pressure distribution on the moving bus, Re=6817, and $\omega_c = U_i$ / r.
e) Flow around the moving bus, Re=6817, and $\omega_c = - U_i$ / r.
f) Pressure distribution on the moving bus, Re=6817, and $\omega_c = - U_i$ / r.

showed that, the cylinder rotation resulted in a slight decrease in the pressure forces on the bus back surface. This reduction in pressure on the back surface of the bus corresponds to increases in the total drag, and these results contradict what was expected. When we investigated the effects of cylinder rotation in the counter-clockwise direction, little increases in the pressure forces appeared. Figure 5 illustrates the flow patterns and the pressure distribution behind the bus for three cases; a fixed cylinder, a cylinder rotating in the counter-clockwise direction, and a cylinder rotating in the clockwise

direction.

For the no rotation case, a weak circulation occurs next to the back surface which may result in a little reduction in the pressure on the back surface. When the cylinder rotates counter-clockwise, the fluid adjascent to the cylinder moves opposite to the flow direction. This motion resulted in a reduction of the main flow velocity in this region and pushing back the circulation bubble to be behind the cylinder. This leads to a weaker circulation next to the cylinder and accordingly, an improvement in the pressure forces on the back surface. When rotating the cylinder in a clockwise direction the fluid speed adjacent to the back surface considerably accelerates and a great portion of the flow energy converts into kinetic energy and accordingly, a reduction in the pressure occurs in this region. Although, part of this kinetic energy again converts into pressure in the lower corner, as shown in Fig. 5.f but, this increase has a little contribution to the total pressure force. When Re=6817, and $\omega_c = U_i / r$ the increase of pressure forces on the bus back surface corresponded to a reduction in the drag of about 7.3%.

*3.2 the Nusselt number*

The air that is flowing downstream the step is used to cool the lower hot wall downstream the step. This heat exchange is expressed by the average wall value of the non-dimensional Nusselt number which is calculated from;

$$\boldsymbol{Nu_{av}} = \frac{\int \boldsymbol{Nu_x}\, \boldsymbol{dx}}{\boldsymbol{L}} \qquad \textbf{(5)}$$

Figure 6 illustrates the variations of the average Nusselt number on the wall downstream the step with the Reynolds number, the cylinder rotation speed, and the cylinder position.

It is observed that, for all shown cases, the Nusselt number increases with the Reynolds number. For all the Reynolds number values the case, H=0.5 S, exhibited the highest values of Nusselt number, and the case, H=1.0S, exhibited the lowest Nusselt values. The results of the case H=1.5S were between the fore-mentioned two cases. That may be because, for the case, H=0.5S, the circulation next to the step produce downward flow that faces the cylinder, and the interaction between them produces large scale vortices that stretch smaller-scale vortices while moving in the downstream direction. The destruction of these vortices results in an increase in the turbulence intensity over the wall, which in turn, improves the mixing and increases the transport of the thermal energy. Increasing the cylinder height produces a larger region between the step and the cylinder which reduces the interaction between the circulation next to the step and the flow around the cylinder. These conditions reduce the possibilities of vortices formation and accordingly produces a lower turbulence intensity. Raising the cylinder to height, H=1.5S produces the largest passage between the step and the cylinder and the small cylinder size produces almost no separation zone behind it. So, the step is almost the only source of circulations which has lower turbulent intensity due to the low possibilities of interaction with the surrounding flow. The weak vortices produced from these circulations decay during moving in the downstream direction. Thus, the transport of thermal energy achieves the lowest value in this case.

In all cases, the effect of cylinder rotation in the counter-clockwise direction is to produce a flowing stream that opposes the gross flow and the interaction between them increases the turbulent transport of the thermal energy.

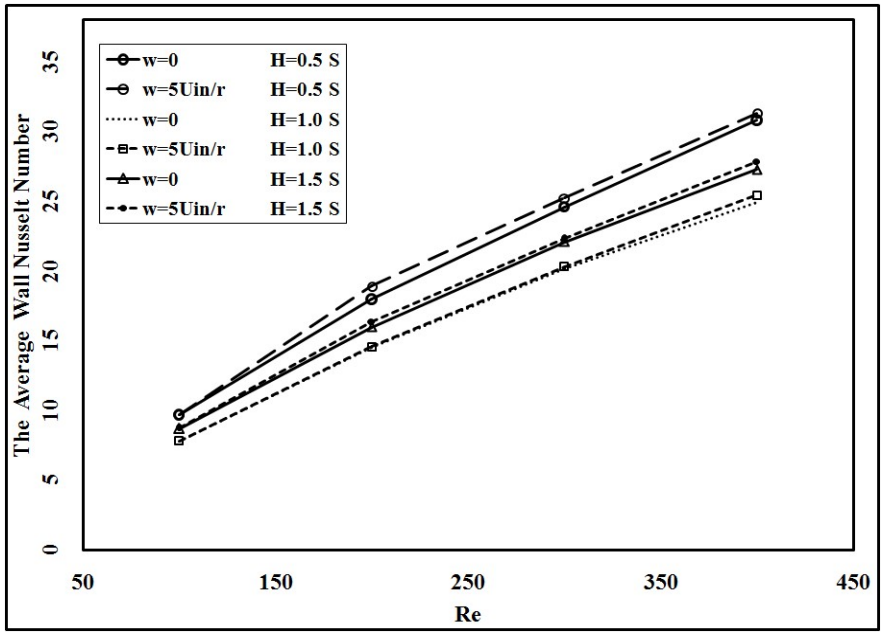


Fig. 6 the variations of the average Nusselt number on the wall downstream the step.

## IV. CONCLUSIONS

It is required to investigate the heat transfer and the drag on the surfaces of some specified cases after moving parts of these surfaces with different values of Reynolds numbers, different cylinder rotation speeds, and different cylinder positions. When rotating a cylinder next to a backward-facing step, a maximum local Nusselt number value of 31.3 could be achieved at Reynolds number, Re, equals 400, when the cylinder is at height H, that equals half the step height, S and is rotating counterclockwise at rim speed, ω r, that equals five times the inlet velocity, $U_i$. The nondimensional force on the step in the opposite flow direction achieved a maximum value of -0.103 with Re=400, H=1.0 S, and ω r=5 $U_i$. When rotating a cylinder in the upper corner of a simulated bus, the drag was reduced by 7.3% when Re=6817, and $\omega_c = U_i / r$.

## REFERENCES

[1] Adib Bazgir and Nader Nabhani, Computational fluid dynamics comparison of separation performance analysis of uniform and non-uniform counter-flow Ranque-Hilsch Vortex Tubes (RHVTs). International Journal of Heat and Technology Vol. 36, No. 2, June 2018, pp. 643-656. DOI:https://doi.org/10.18280/ijht.360229.

[2] Aditya Mushyam and Josep M Bergada, Active Flow Control on Laminar flow over a Backward facing step, 4th International Conference on Mathematical Modeling in Physical Sciences (IC-MSquare2015) IOP Publishing Journal of Physics: Conference Series 633 (2015) 012110 doi:10.1088/1742-6596/633/1/012110.

[3] B. F. Armaly, F. Durst, J. C. F. Pereira, and B. Schönung, Experimental and theoretical investigation of backward-facing step flow, Journal of Fluid Mechanics, Volume 127, February 1983, pp. 473-496.

[4] C. Choveta, M. Lipperta , L. Keirsbulcka , and J-M. Foucautb, Unsteady behavior of separated and reattaching flows for a backward-facing step configuration at high Reynolds, 23ème Congrès Français de Mécanique Lille, 28 au 1cr September 2017.

[5] Dwight Barkley, M. Gabriela, M. Gomes, and Ronald D. Henderson, Three-dimensional instability in flow over a Backward-Facing Step, J. Fluid Mech. (2002), vol. 473, pp. 167–190. c 2002 Cambridge University Press DOI: 10.1017/S002211200200232X.

[6] F. Durst and C. Tropea, Flows over Two-Dimensional Backward-Facing Steps, Structure of Complex Turbulent Shear Flow, Symposium, Marseille, France August 31 – September 3, 1982, pp 41-52.

[7] F. Durst and J. C. F. Pereira, Time-Dependent Laminar Backward-Facing Step Flow in a Two-Dimensional Duct, J. Fluids Eng. Sep 1988, 110(3): 289-296 (8 pages), https://doi.org/10.1115/1.3243547.

[8] Fang-fangWang, Shi-qiangWu, Sen-linZhu, Numerical simulation of flow separation over a backward-facing step with high Reynolds number, Water Science and Engineering, Volume 12, Issue 2, June 2019, Pages 145-154.

[9] H. Lan, B. F. Armaly, and J.A.Drallmeier, Three-dimensional simulation of turbulent forced convection in a duct with backward-facing step, International Journal of Heat and Mass Transfer Volume 52, Issues 7–8, March 2009, Pages 1690-1700, DOI: 10.1016/j.ijheatmasstransfer.2008.09.022.

[10] K. Slim, S. OPark, and H. SShim, A low aspect ratio backward-facing step flow, Experimental Thermal and Fluid Science, Volume 3, Issue 5, September 1990, Pages 508-514, https://doi.org/10.1016/0894-1777(90)90064-E

[11] Hayette Djedai, Ramzi Mdouki, Zakaria Mansouri, and Mokhtar Aouissi, Numerical investigation of three-dimensional separation control in an axial compressor cascade, International Journal Of Heat And Technology, Vol. 35, No. 3, September 2017, pp. 657-662, DOI: 10.18280/ ijht.350325.

[12] Hoi Hyun Choi, Van Thinh Nguyenb, and John Nguyen, Numerical Investigation of Backward Facing Step Flow over Various Step Angles, Procedia Engineering 154 (2016) 420 – 425 1877-7058 © 2016, Doi: 10.1016/j.proeng.2016.07.508, ScienceDirect Available online at www.sciencedirect.com 12th International Conference on Hydroinformatics, HIC 2016.

[13] Lin Chen, Keisuke Asai, Taku Nonomura, Guannan Xi, and Tianshu Liu, a review of Backward-Facing Step Flow mechanisms, heat transfer and control, Thermal Science and Engineering ProgressVolume 6, June 2018, Pages 194-216, https://doi.org/10.1016/j.tsep.2018.04.004.

[14] Pankaj Srivastava, Anupam Dewan, and Jugal K. Bajpai, Flow and heat transfer characteristics in a convergent-divergent shaped microchannel with ribs and cavities, International Journal of Heat and Technology, December 2019, pp. 863-873, DOI:https://doi.org/10.18280/ijht.350423.

[15] Raheem K. Ajeel, Wan S., W. Salim, and Khalid Hasnan, Numerical investigations of flow and heat transfer enhancement in a semicircle zigzag corrugated channel using nanofluids, International Journal of Heat and Technology, December 2018, pp: 1292-1303, DOI: https://doi.org/10.18280/ijht.360418.

[16] Seyed Ehsan Rafiee and M. M. Sadeghiazad, Heat and Mass Transfer Between Cold and Hot Vortex Cores inside Ranque-Hilsch Vortex Tube-Optimization of Hot Tube Length, International Journal of Heat and Technology, Vol. 34, No. 1, March 2016, pp. 31-38, DOI: 10.18280/ijht. 340105.

[17] Seyed Ehsan Rafiee and M. M. Sadeghiazad, Venkatesh Saravanan, Chitradurga K. Umesh, Doddamani Hithaish, and Kanakanahalli Seetharamu, Numerical investigation of pressure drop and heat transfer in pin fin heat sink and micro channel pin fin heat sink, International Journal of Heat and Technology Vol. 36, No. 1, March 2018, pp. 267-276, https://doi.org/10.18280/ijht.360136.

## Nomenclature

### Alphabetic

| | | |
|---|---|---|
| A | area | $m^2$. |
| h | heat transfer coefficient | $W/(m^2.K)$. |
| k | thermal conductivity | W/(m .K). |
| Nu | Nusselt number | |
| r | cylinder radius | m. |
| Re | Reynolds number | |
| U | air velocity | $m.s^{-1}$. |

### Subscripts

| | |
|---|---|
| av | average. |
| D | drag. |
| f | form. |
| i | inlet. |
| s | skin. |
| x | x_coordinate. |

### Greek Symbols

| | | |
|---|---|---|
| μ | dynamic viscosity | Pascal.s. |
| ρ | density | $kg/m^3$. |
| ω | cylinder angular velocity | rad/s. |